ACTA IMEKO
ISSN: 2221-870X
September 2024, Volume 13, Number 3, 1 - 7

Quality control of 3D printing in bioarchaeology: a case study on dimensional assessment of cranial models

Marta Cecchitelli[1,2], Giorgia Fiori[1], Gabriele Bocchetta[1], Federico Filippi[1], Fabio Leccese[3], Jan Galo[2], Salvatore Andrea Sciuto[1], Andrea Scorza[1]

[1] *Department of Industrial, Electronic and Mechanical Engineering, Roma Tre University, Via della Vasca Navale 79, 00146 Rome, Italy*
[2] *IRCCS Children Hospital Bambino Gesù, Piazza di Sant'Onofrio 4, 00165 Rome, Italy*
[3] *Department of Science, Roma Tre University, Viale Guglielmo Marconi 446, 00146 Rome, Italy*

ABSTRACT
In the last few years, 3D printing has gained widespread use in archaeology and cultural heritage fields, from research and conservation to enriching museum experiences. This study focuses on Fused Deposition Modeling (FDM) technology to assess the quality of printed replicas of archaeological human remains. A cranial model was 3D printed (3DP) from Computed Tomography (CT) data of an 8-year-old patient to simulate the remains of an archaeological skull. Eight copies were then printed and subjected to CT scanning to compare them to the original model through an objective measurement method based on image analysis. The proposed method investigates print variability and considers potential sources of error to assess the dimensional compatibility of the model before and after printing. Results showed an increasing error, up to 15 %, with higher levels of model detail. These results are discussed with reference to a metrological approach, highlighting the need for further research into optimizing 3D printing quality control, including through the definition of a standardized protocol to obtain archaeological replicas faithful to the originals.

Section: RESEARCH PAPER

Keywords: 3D printing; fused deposition modeling; quality control; cranial model; CT scanning

Citation: M. Cecchitelli, G. Fiori, G. Bocchetta, F. Filippi, F. Leccese, J. Galo, S. A. Sciuto, A. Scorza, Quality control of 3D printing in bioarchaeology: a case study on dimensional assessment of cranial models, Acta IMEKO, vol. 13 (2024) no. 3, pp. 1-7. DOI: 10.21014/actaimeko.v13i3.1828

Section Editor: Francesco Lamonaca, University of Calabria, Italy

Received February 28, 2024; **In final form** June 9, 2024; **Published** September 2024

Corresponding author: Marta Cecchitelli , e-mail: marta.cecchitelli@uniroma3.it

1. INTRODUCTION

Three-dimensional (3D) printing has seen broad adoption in archaeology and cultural heritage fields: its versatility extends to various applications, including research, conservation, and enhanced museum experiences [1].

The 3D archives in museums (e.g., physical model, 3D printed model, simulated reconstruction) enable the preservation of features of finds and human remains to ensure their display. In this way, the archaeological specimen, often already deteriorated, can be protected without compromising its integrity. Museums are increasingly incorporating tactile experiences into their exhibits, providing visitors with opportunities to engage with artifacts beyond visual inspection. Touchable exhibitions and handling sessions let to connect with objects: 3D printed (3DP) replicas of original finds allow visitors to physically interact with them [2]. Moreover, 3D printing has proven to be a valid tool for the inclusive valorisation of cultural heritage supporting individuals with visual, cognitive, or sensory-perceptual disabilities to engage with it [3].

3D printing enables archaeologists to create detailed replicas of artifacts and structures, allowing them to study features and reconstruct ancient environments without risking damage to the original objects. It can also be used to repair damaged objects, providing a minimally invasive alternative to traditional restoration methods [4], [5].

Both the preservation of minimal details and the study of fragile artifacts have been revolutionized by non-destructive techniques such as Computed Tomography (CT) and rapid prototyping. In the field of archaeology, their most important application lies in the exploration of ancient Egyptian mummies [6], [7]. 3D printing has potential in the field of mummy studies, particularly in visualizing skeletal and anomalous inclusions within wrapped bundles of mummies. In [8], clinical imaging and 3D printing have been used for the identification of anomalies in an ancient animal mummy, while a 3D printed model of an

ancient falcon mummy skeleton has been reproduced in [9]. In [10], the usefulness of this practice has been shown through a qualitative evaluation of the 3D printed models for ancient species identification.

In [11], a novel 3D segmentation and model reconstruction has been carried out on CT images of the heart and liver obtained from a Gangneung mummy of the Joseon dynasty. Based on the promising results, the future potential of this technique in paleopathological research without tissue destruction has been evaluated. In this regard, a further application of modern 3D technologies in the field of archaeology is disease analysis, which allows for a deeper understanding of the history of diseases and their impact on human populations over time. In [12], the importance of using an analytical approach to paleopathology that incorporates up-to-date CT and 3D imaging techniques has been highlighted, particularly for the diagnosis of metastatic cancer in an Iron Age skull. Specimens can be physically reproduced by 3D printing using techniques developed in the biomedical field [13] to study anatomy and paleopathology from archaeological remains. CT scanning and 3D printing allow the internal anatomical surfaces of bone remains to be analysed and reproduced [14]. Special attention is paid to the reconstruction and 3D visualization of skulls because they are sources of numerous historical and anthropological information on human remains such as the estimation of age-at-death using teeth or cranial sutures [15], [16]. In [17], the skull of an interesting archaeological case showing severe pathological changes has been CT-scanned, and replicas of all the single bones 3D printed and manually re-assembled to overcome the taphonomic alterations providing important diagnostic information.

The 3D reconstruction technology is a powerful solution for studying inaccessible archaeological specimens, such as the remarkable Neanderthal skeleton discovered near Altamura, Italy in 1993 [18]. Located in a narrow cave passage with limited access, the Altamura Neanderthal skeleton was deemed too delicate to be removed from its original site for study. The 3D reconstruction of the cranium provided a non-invasive alternative to the examination of the skeleton's anatomy, revealing previously hidden features and providing valuable insights into the Neanderthal evolution [18]. Despite the growing interest in Virtual Anthropology [19], and the advancements in 3D printing technology, there are currently no standardized quality controls for 3D printed models in the anthropological field [20]. This stands in contrast with the regulated environment of the biomedical field, where 3D printed models used for clinical purposes are considered medical devices and must adhere to strict guidelines [21], [22]. Without standardized quality control, there is a risk of inaccuracies and inconsistencies in the representation of archaeological and anthropological artifacts. Therefore, to ensure the reliability of 3D printed models, it is necessary to develop clear guidelines and standards for quality control. A standardized approach ensures trustworthiness and reproducibility from data acquisition and digitization to model creation and validation [23]. In a study of human remains from the Neolithic Age discovered in the Tyrolean Alps in 1991, the truthfulness of a 3D skull reconstruction has been validated by comparing measurements from the original CT images to external physical measurements of the intact head of the mummy [24]. The validation procedure demonstrated the critical importance of checking virtual reconstructions to ensure their faithfulness and reliability to the original archaeological specimens.

Based on the considerations above, this study would provide a novel contribution to the field by proposing a quantitative dimensional analysis for 3D printing quality control in bioarchaeology to check that 3D printed models reflect the original archaeological specimens. In particular, it is a novel approach from a metrological point of view, previously proposed in [25], which aims at providing a rigorous method for evaluating the accuracy of 3D printed models representing archaeological human remains, considering the main possible error sources. Specifically, the study focuses on a more thorough estimation of the uncertainty of the method in [25] that assesses the dimensional compatibility between data acquired from a CT examination of a 3D printed model simulating an archaeological human skull and CT data of eight replicas of the same model, all produced using Fused Deposition Modeling (FDM) technology.

In Section 2, we will describe the materials and the printing protocol used, the supporting techniques, and tools involved. The method developed to conduct the dimensional comparison is given in detail, explaining the objective image analysis method implemented. Next, we will dedicate Section 3 to analysing the measurement uncertainty associated with the results, focusing on the uncertainty contributions considered and clarifying how they were estimated and combined together. In Section 4 the results, reported in tabular form, are discussed and commented investigating the possible variability introduced by the printing process and highlighting the most significant observations. Finally, in the last section, potential applications and improvements of the developed method contributing to the broader field of 3D printing are outlined.

2. MATERIALS AND METHODS

For the sake of this study, a cranial model serving as a simulated archaeological specimen was 3D printed. This skull specimen was realized from the CT data (Siemens Somatom Force® dual source tomograph [26]) of an anonymous diagnostic examination performed on an 8-year-old patient. The anonymized data were obtained in accordance with ethical guidelines for medical research [27], [28]. This simulated specimen served as the gold standard against which its replicas were compared.

The Digital Imaging and Communications in Medicine (DICOM) dataset was imported into a specialized medical 3D image segmentation software, i.e., Mimics Materialise 25.0 (Leuven, Belgium) [29]. The digital segmentation was accomplished using a semi-automated technique. The initial step involved automatic thresholding based on Hounsfield Units (HU) ranging from –802 HU to +647 HU, tailored for all models. Subsequently, smart fill and smart brush tools were used

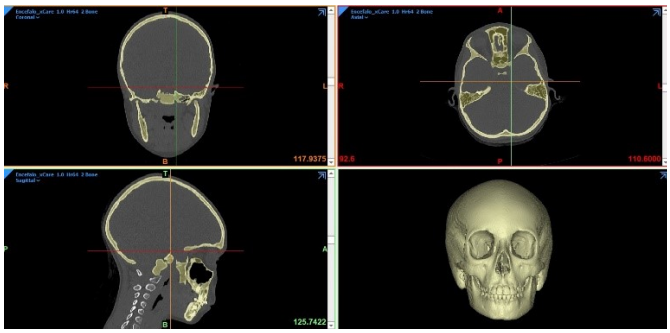

Figure 1. 3D reconstruction of the skull from axial, coronal and sagittal views from the CT examination.

Figure 2. Gold standard model to be printed and assumed as a simulated archaeological specimen.

to refine the 3D model, mimicking typical clinical workflow. To ensure that the 3DP model was suitable for the reference purpose, the 3D reconstruction of the skull from CT images (Figure 1) was exported to Autodesk Meshmixer and subjected to manual smoothing to remove surface blemishes and irregularities. The smoothing process was carried out using the "shape preserving" tool with a smoothing factor set to 1.

To reduce the use of material and printing time, while preserving anatomical details, the skull model was scaled down to 75 % of its original size. The segmented object was exported to Medical 3-matic 17.0 and converted to an optimized STL file (Figure 2), minimizing artifacts such as stitching, holes and overlaps, suitable for the print file (.3mf). These corrective operations were automatically carried out using the Auto Fix tool in Medical 3-matic to enhance the integrity of the model. The .3mf file was then processed using UltiMaker Cura 5.2.2 to generate the G-code for printing. The gold standard model, referred to as Skull0, was printed on UltiMaker S5 Pro Bundle printer [30] (Figure 3) using the same printing parameters as the eight replicas, except for a slightly lower layer thickness to ensure optimal surface quality (Table 1). All 3D models were printed in polylactic acid (PLA, extruder 1 in Table 1), a material widely used with FDM technology [31], which exhibits excellent CT compatibility, mimicking the response of the bone to X-rays without luminescence artifacts. To facilitate the printing process, a water-soluble support structure made of polyvinyl alcohol (PVA, extruder 2 in Table 1) [32] was automatically generated for all 3D models. This material is particularly suitable for complex geometries such as the skull, ensuring easy removal and minimal interference between contact surfaces, a critical factor for accurate dimensional measurements. The support structure was designed to maintain a 45° overhang angle, minimizing material usage and ensuring structural integrity.

Figure 3. Cranial model 3D printing with UltiMaker S5 Pro Bundle.

Table 1. Main printing parameters.

Parameter	Extruder 1	Extruder 2
Material	PLA	PVA
Print temperature	205 °C	220 °C
Print speed	40 mm·s^{-1}	35 mm·s^{-1}
Layer height: eight replicas	0.2 mm	0.2 mm
Layer height: Skull0	0.1 mm	0.1 mm
Infill density	10 %	-

Upon completion of printing and post-processing, the gold standard 3DP cranial model underwent a high-resolution CT scan. The scanning protocol was followed meticulously according to the specifications listed in Table 2. Acquired CT images were segmented using thresholding techniques to extract anatomical features for subsequent replica printing. Eight 3D replicas were produced using the same printing parameters as the gold standard, except for manual smoothing operations to maintain consistent production methods. The software used for image analysis and segmentation is designed specifically for biomedical applications and operates on CT images in Hounsfield Units (HU). The latter are dimensionless values universally employed in CT scanning to quantify the radiodensity of anatomical structures [33]. These values are linearly correlated with the grayscale of CT images [34], providing a direct and quantifiable measure of tissue density.

To ensure a standardized and consistent method, all segmented 3D models were processed using a custom threshold range of -802 to 739 HU, specifically selected based on the x-ray response of the gold standard PLA. Segmented objects were automatically wrapped and smoothed several times with identical settings to maintain uniformity. All segmented models were imported into Medical 3-matic 17.0 to optimise the mesh and save the STL files for printing. The STL files were then imported into UltiMaker Cura 5.2.2 for G-code generation according to the parameters in Table 1. The nine 3D cranial models, i.e., the gold standard Skull0 and its replicas, were subjected to the same CT scanning protocol to allow direct comparison of their dimensional measurements. Figure 4 shows the eight replicas, arranged with Skull0.

To maintain consistency in positioning, all skulls were scanned following the paediatric head CT protocol. They were carefully placed in a dedicated stand (Figure 5) and centred within the gantry using a cruciform laser system (Figure 6). To ensure repeatability, a single experienced radiology technician was responsible for positioning all skulls.

Table 2. Main CT scanning protocol settings.

CT parameter	Value
Total number of slices	263
Slice thickness	0.5 mm
Slice increment	0.5 mm
Pixel size	0.35 × 0.35 mm^2
Field of view	180 mm
Voltage peak	90 kV
Single collimation width	0.59 mm
Step factor	0.55

Figure 4. Skull0 in front and its eight replicas behind.

A rigorous and objective method based on image analysis was applied to assess the dimensional congruence between the gold standard Skull0 and its replicas. This method involves automatic segmentation of CT scans to identify the slice with the largest outer diameter for each skull, enabling 2D analysis. The segmentation of CT images, based on a threshold value derived from the grayscale values of the data acquired, allows determining 3D masks for all skulls. The slice corresponding to the mask with the largest outer diameter is identified for replicas and Skull0 and used for the dimensional comparison based on the following quantitative parameters (Figure 7): section area (A), maximum longitudinal diameter (D_{max}), and thicknesses identified at the latter (S_1 and S_2). These measurements are compared for each replica and the Skull0, resulting in the quantitative values and the percentage difference (Δ) of the above quantities. Specifically, A is determined by counting the white pixels in the selected mask and then converting the pixel count to mm² based on pixel size (Table 2).

Figure 5. 3DP cranial model placed in the dedicated stand for CT scan.

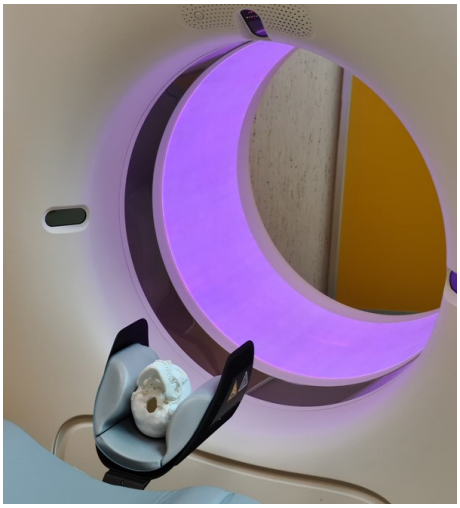

Figure 6. Cranial model centred within the gantry using a cruciform laser system.

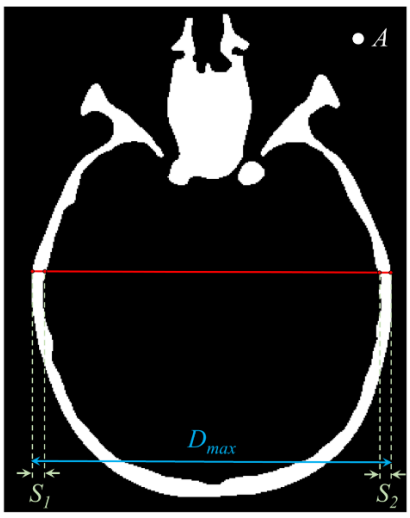

Figure 7. Mask of the CT slice in which the measured quantities being compared are shown. A: area of skull section (white pixels); D_{max}: maximum longitudinal diameter; S_1 and S_2: skull thicknesses at D_{max}.

3. UNCERTAINTY ANALYSIS

A comprehensive uncertainty analysis was carried out considering the following sources of error. The uncertainty in the pixel resolution of CT images was evaluated by considering the pixel size shown in Table 2. The uncertainty contribution associated with the image analysis method was evaluated using a Monte Carlo (MC) simulation [35]-[41] with 10^4 iterations. As listed in Table 3, the grayscale threshold value for the automatic assessment of the 3D masks was varied randomly within a rectangular distribution of ± 5 % bounds. Compared to the previous study [25], the variability stemming from operator-dependent skull positioning errors during CT acquisition was introduced and included in the same MC simulation. This contribution was considered by randomly varying the identification of the slice with the maximum diameter, admitting an error of at most two slices (Table 3).

To obtain a first estimate of the overall measurement uncertainty, the two uncertainty contributions, due to pixel resolution and image analysis, were combined using the uncertainty propagation law.

Table 3. Summary table of the distributions used to calculate the contribution of uncertainties in the Monte Carlo simulation.

Type of uncertainty	Distribution	Setting
Thresholding	Rectangular	500 ± 5 % bounds
Positioning	Rectangular	slice at D_{max} ± 1 bounds

Table 4. Dimensional measurements (*mean* ± *SD*) on the model mask.

3DP model	A (mm²)	D_{max} (mm)	S_1 (mm)	S_2 (mm)
Skull0	2054 ± 12	101.1 ± 0.2	4.1 ± 0.2	3.9 ± 0.2
Skull1	2192 ± 32	101.4 ± 0.2	4.0 ± 0.3	4.4 ± 0.3
Skull2	1900 ± 13	101.0 ± 0.2	4.2 ± 0.2	4.5 ± 0.2
Skull3	2206 ± 9	101.2 ± 0.3	4.3 ± 0.2	4.6 ± 0.2
Skull4	2089 ± 34	101.0 ± 0.2	4.4 ± 0.3	4.0 ± 0.3
Skull5	2111 ± 7	99.7 ± 0.3	4.5 ± 0.2	3.9 ± 0.2
Skull6	1876 ± 4	101.0 ± 0.4	4.1 ± 0.2	4.5 ± 0.2
Skull7	1971 ± 12	101.6 ± 0.2	4.2 ± 0.2	4.0 ± 0.2
Skull8	2176 ± 68	101.6 ± 0.2	3.9 ± 0.4	4.2 ± 0.2

Table 5. Differences in dimensional measurements (*mean* ± *SD*) between model masks.

3DP model	A (%)	D_{max} (%)	S_1 (%)	S_2 (%)
$\Delta_{1,0}$	3.63 ± 0.06	0.32 ± 0.01	6.7 ± 1.8	3.0 ± 0.9
$\Delta_{2,0}$	7.51 ± 0.07	0.05 ± 0.01	10.6 ± 1.9	9.0 ± 1.6
$\Delta_{3,0}$	7.37 ± 0.05	0.22 ± 0.01	11.5 ± 2.7	11.4 ± 2.3
$\Delta_{4,0}$	1.68 ± 0.03	0.13 ± 0.01	3.5 ± 1.1	14 ± 4
$\Delta_{5,0}$	2.75 ± 0.02	1.38 ± 0.01	6.2 ± 1.4	17 ± 3
$\Delta_{6,0}$	8.67 ± 0.05	0.26 ± 0.01	8.9 ± 2.2	6.5 ± 1.5
$\Delta_{7,0}$	4.07 ± 0.03	0.56 ± 0.01	2.2 ± 0.4	9.1 ± 2.3
$\Delta_{8,0}$	5.93 ± 0.19	0.56 ± 0.01	3.3 ± 1.3	0.3 ± 0.1

4. RESULTS AND DISCUSSION

The measurements obtained for each replica and the Skull0, specifically section area (A), maximum longitudinal diameter (D_{max}), and thicknesses (S_1 and S_2) resulted in the quantitative values listed in Table 4 and in the differences (Δ), expressed as percentages in Table 5. Table 4 shows the dimensional results for each skull at the slice with the maximum longitudinal diameter. Conversely, Table 5 presents the results of comparing each skull with Skull0 in terms of percentage discrepancy ($\Delta_{i,0}$). This value represents the relative differences between the i-th skull and Skull0, where $i = 1, 2, \ldots, 8$. The results are expressed as mean ± standard deviation (SD).

A general observation from the dimensional measurements, excluding area values, revealed that pixel resolution is the primary source of uncertainty. In fact, the standard deviation associated with the image analysis procedure is usually significantly lower (about an order of magnitude) than that attributed to pixel size, except for some specific cases discussed below. In particular, for D_{max} of Skull6 and S_1 for Skull8 the contributions of pixel resolution and image analysis uncertainty appear comparable.

While considering additional error sources, the variation in average parameter values seems to be justified by the variability inherent in the printing process and the limitations of the whole technological process, starting from the slicing phase of the 3D mathematical model. Indeed, the percentage error between the gold standard and the replicas increases as the level of detail in the object intensifies. The maximum discrepancy observed in the macroscopic parameter (D_{max}) is approximately 1 %, while an error exceeding 15 % is obtained for the two thicknesses.

In addition, the variability found in S_1 and S_2 thicknesses is consistent with the uncertainty arising from the printing process. The printer nozzle has a diameter of 0.4 mm, and depending on the number of layers deposited, there is a variability multiple of 0.4 mm in the mean thickness value. The Δ values, expressed as the percentage difference between the compared thicknesses, indicate the extent to which the printer deposited more or fewer layers in the section under consideration. This is reflected in the percentage error between the thickness of the gold standard model and its replicas (Table 5): the relative uncertainty associated with the discrepancies is about one percentage point.

Despite the attempt to quantify errors due to model placement within the CT, the spread of results in terms of both mean value and standard deviation obtained for the areas suggests that the section with the maximum longitudinal diameter may differ between Skull0 and its replicas. Area measurements diverge in the slice range in which the anatomical geometry of the orbits and sinuses varies, leading to variability in the cross-sectional area value. However, the maximum diameter and thicknesses remain consistent. This is likely due to the repeatability of skull positioning during CT data acquisition.

5. CONCLUSIONS

This study focused on 3D printing quality assessment for archaeological and cultural heritage applications. Specifically, the use of 3D printing for replicating findings and human remains requires a rigorous approach to ensure the accuracy of 3D replicas. Despite considerable interest in the topic, further metrological investigations are needed to establish effective quality control of 3D printed models. In this regard, the present study proposes an objective measurement method based on image analysis processing to carry out dimensional comparisons between an archaeological specimen and its replicas.

To simulate human remains, a three-dimensional cranial model was reconstructed from CT data acquired from a human skull. This model, serving as the gold standard, was 3D printed using FDM technology and CT scanned with a high-resolution protocol. The resulting dataset was segmented to generate eight 3DP replicas, which were then subjected to dimensional comparison with the gold standard model. This study represents a case study on the quality assessment of 3D printing, demonstrating the suitability of 3DP replicas for museum exhibition purposes, given their minimal dimensional discrepancies (within a few percentage points). However, further investigations are needed to better understand the factors influencing replica accuracy. The measurement results suggest that the dispersion of differences between the replicas and the reference skull is due to two primary sources: printing process variability and method uncertainty. Based on the outcomes of this study, further research on method repeatability needs to be carried out to explore the impact of printing process variability alone. In this case, investigating the potential for error introduced during the manual positioning of 3DP models by radiology technicians is crucial to fully understanding the sources of dimensional discrepancies.

Based on these considerations, additional investigations are warranted to address various issues of dimensional assessment in 3D printing. Firstly, expanding the scope of dimensional measurements to include volume assessment from all CT slices would provide a more comprehensive assessment of the replica. Moreover, dimensional verification on a larger number of samples, varying both the 3D model geometry and the printing parameters, would establish acceptable tolerance ranges for ensuring the quality of 3D printed replicas. Finally, examining the dimensional congruence of 3D replicas produced by different printing technologies, e.g., stereolithography and selective laser sintering, would provide insights into the technology-specific effects on dimensional accuracy.

In the future, the proposed protocol could be refined and applied to the study of mummies and archaeological remains of historical significance, fostering a deeper understanding of their anatomical characteristics and cultural contexts.

REFERENCES

[1] M. Neumüller, A. Reichinger, F. Rist, C. Kern, 3D printing for cultural heritage: preservation, accessibility, research and education, in: 3D Research Challenges in Cultural Heritage. Lecture Notes in Computer Science, vol. 8355. M. Ioannides, E. Quak (editors). Springer, Berlin, Heidelberg, 2014, ISBN 978-3-662-44630-0, pp.119-134.
DOI: 10.1007/978-3-662-44630-0_9

[2] M. Ballarin, C. Balletti, P. Vernier, Replicas in cultural heritage: 3D printing and the museum experience, Int. Arch. Photogramm. Remote Sens. Spatial Inf. Sci. XLII-2 (2018), pp. 55-62.
DOI: 10.5194/isprs-archives-XLII-2-55-2018

[3] E. Rossi, P. Barcarolo, Use of digital modeling and 3D printing for the inclusive valorization of cultural heritage, in: Advances in Manufacturing, Production Management and Process Control. AHFE 2018. Advances in Intelligent Systems and Computing, vol. 793. W. Karwowski, S. Trzcielinski, B. Mrugalska, M. Di Nicolantonio, E. Rossi (editors). Springer Cham, 2019, ISBN 978-3-319-94196-7, pp. 257-269.
DOI: 10.1007/978-3-319-94196-7_24

[4] L. Acke, K. De Vis, S. Verwulgen, J. Verlinden, Survey and literature study to provide insights on the application of 3D technologies in objects conservation and restoration, J. Cult. Herit. 49 (2021), pp. 272-288.
DOI: 10.1016/j.culher.2020.12.003

[5] Y. Zhou, E. Aura-Castro, E. Nebot Díaz, 3D printing technology and its application in the conservation and restoration of porcelain, ISPRS Ann. Photogramm. Remote Sens. Spatial Inf. Sci. X-M-1-2023 (2023), pp. 301-307.
DOI: 10.5194/isprs-annals-X-M-1-2023-301-2023

[6] E. B. Yatsishina, S. V. Vasilyev, O. A. Vasilieva, R. M. Galeev, O. P. Dyuzheva, M. V. Kovalchuk, CT-scanning analysis of the inner structure of ancient Egyptian mummy, Crystallogr. Rep. 65 (2020), pp. 1064-1072.
DOI: 10.1134/S1063774520060401

[7] C. Villa, J. Davey, P. J. G. Craig, O. H. Drummer, N. Lynnerup, The advantage of CT scans and 3D visualizations in the analysis of three child mummies from the Graeco-Roman period, Anthropol. Anz. 72 (2015) 1, pp. 55-65.
DOI: 10.1127/anthranz/2014/0330

[8] L. M. McKnight, J. E. Adams, A. Chamberlain, S. D. Atherton-Woolham, R. Bibb, Application of clinical imaging and 3D printing to the identification of anomalies in an ancient Egyptian animal mummy, J. Archaeol. Sci. Rep. 3 (2015), pp. 328-332.
DOI: 10.1016/j.jasrep.2015.06.028

[9] A. Du Plessis, R. Slabbert, L. C. Swanepoel, J. Els, G. J. Booysen, S. Ikram, I. Cornelius, Three-dimensional model of an ancient Egyptian falcon mummy skeleton, Rapid Prototyp. J. 21 (2015) 4, pp. 368-372.
DOI: 10.1108/RPJ-09-2013-0089

[10] R. Bibb, L. McKnight, Identification of bird taxa species in ancient Egyptian mummies: part 2, a qualitative evaluation of the utility of CT scanning and 3D printing, J. Archaeol. Sci. Rep. 46 (2022).
DOI: 10.1016/j.jasrep.2022.103668

[11] E. Koh, D. Y. Lee, D. Yoo, M. J. Kim, J. H. Hong, S. J. Park, J. Kim, I. S. Lee, D. H. Shin, Three-dimensional reconstruction of Gangneung mummy's heart and liver based on the computed tomography images, Anc. Asia 14 (2023), pp. 1-8.
DOI: 10.47509/AA.2023.v14i.01

[12] R. Miccichè, G. Carotenuto, L. Sineo, The utility of 3D medical imaging techniques for obtaining a reliable differential diagnosis of metastatic cancer in an iron age skull, Int. J. Paleopathol. 21 (2018), pp. 41-46.
DOI: 10.1016/j.ijpp.2017.03.006

[13] Z. Al-Dulimi, M. Wallis, D. K. Tan, M. Maniruzzaman, A. Nokhodchi, 3D printing technology as innovative solutions for biomedical applications, Drug. Discov. Today 26 (2021) 2, pp. 360-383.
DOI: 10.1016/j.drudis.2020.11.013

[14] A. Profico, S. Schlager, V. Valoriani, C. Buzi, M. Melchionna, A. Veneziano, P. Raia, J. Moggi-Cecchi, G. Manzi, Reproducing the internal and external anatomy of fossil bones: two new automatic digital tools, Am. J. Phys. Anthropol. 166 (2018) 4, pp. 979-986.
DOI: 10.1002/ajpa.23493

[15] M. Vystrčilová, V. Novotný, Estimation of age at death using teeth, Variability and Evolution 8 (2000), pp. 39-49.

[16] K. L. Boyd, C. Villa, N. Lynnerup, The use of CT scans in estimating age at death by examining the extent of ectocranial suture closure, J. Forensic Sci. 60 (2015) 2, pp. 363-369.
DOI: 10.1111/1556-4029.12683

[17] A. A. Lundquist, N. D. Jensen, M. L. Jørkov, N. Lynnerup, C. Villa, How 3D printing and physical reconstruction of a skull helped in a complex pathological case, Anthropol. Anz. 79 (2022) 1, pp. 83-94.
DOI: 10.1127/anthranz/2021/1270

[18] A. Profico, C. Buzi, F. Di Vincenzo, M. Boggioni, A. Borsato, G. Boschian, D. Marchi, M. Micheli, J. M. Cecchi, M. Samadelli, M. A. Tafuri, J. L. Arsuaga, G. Manzi, Virtual excavation and analysis of the early Neanderthal cranium from Altamura (Italy), Commun. Biol. 6 (2023) 1.
DOI: 10.1038/s42003-023-04644-1

[19] G. W. Weber, Another link between archaeology and anthropology: virtual anthropology, Digit. Appl. Archaeol. Cult. Herit. 1 (2014) 1, pp. 3-11.
DOI: 10.1016/j.daach.2013.04.001

[20] C. Buzi, I. Micarelli, A. Profico, J. Conti, R. Grassetti, W. Cristiano, F. Di Vincenzo, M. A. Tafuri, G. Manzi, Measuring the shape: performance evaluation of a photogrammetry improvement applied to the Neanderthal skull Saccopastore 1, Acta IMEKO 7 (2018) 3, pp. 79-85.
DOI: 10.21014/acta_imeko.v7i3.597

[21] P. Nguyen, I. Stanislaus, C. McGahon, K. Pattabathula, S. Bryant, N. Pinto, J. Jenkins, C. Meinert, Quality assurance in 3D-printing: a dimensional accuracy study of patient-specific 3D-printed vascular anatomical models, Front. Med. Technol. 5 (2023).
DOI: 10.3389/fmedt.2023.1097850

[22] European Medicines Agency, Human regulatory: medical devices. Online [Accessed 18 June 2024]
https://www.ema.europa.eu/en/human-regulatory-overview/medical-devices

[23] L. Fregonese, N. Giordani, A. Adami, G. Bachinsky, L. Taffurelli, O. Rosignoli, J. Helder, Physical and virtual reconstruction for an integrated archaeological model: 3D print and maquette, Int. Arch. Photogramm. Remote Sens. Spatial Inf. Sci. XLII-2/W15 (2019), pp. 481-487.
DOI: 10.5194/isprs-archives-XLII-2-W15-481-2019

[24] D. zur Nedden, R. Knapp, K. Wicke, W. Judmaier, W. A. Murphy Jr, H. Seidler, W. Platzer, Skull of a 5,300-year-old mummy: reproduction and investigation with CT-guided stereolithography, Radiology 193 (1994) 1, pp. 269-272.
DOI: 10.1148/radiology.193.1.8090905

[25] M. Cecchitelli, G. Fiori, G. Bocchetta, F. Filippi, F. Leccese, J. Galo, S. A. Sciuto, A. Scorza, Dimensional assessment in bioarchaeology applications: a preliminary study on quality controls in 3D printing of human skulls, Proc. of the IMEKO TC4 International Conference on Metrology for Archaeology and Cultural Heritage, Rome, Italy, 19 – 21 October 2023, pp. 98-103.
DOI: 10.21014/tc4-ARC-2023.020

[26] Siemens Healthineers, SOMATOM Force. Online [Accessed 18 June 2024]
https://marketing.webassets.siemens-healthineers.com/1800000007576223/e8c8a13a1dbe/siemens-healthineers_ct_somatom_force_8pager_1800000007576223.pdf

[27] H. Kikuchi, S. Ito, K. Ikegami S. Shindo, Diseases prediction from officially anonymized medical and healthcare big data, Proc. of the 2022 IEEE International Conference on Big Data (Big Data), Osaka, Japan, 17 – 20 December 2022.
DOI: 10.1109/BigData55660.2022.10075547

[28] J. A. Onofrey, L. H. Staib, X. Papademetris, Segmenting the brain surface from CT images with artifacts using locally oriented appearance and dictionary learning, IEEE Trans. Med. Imaging 38 (2019) 2, pp. 596-607.
DOI: 10.1109/tmi.2018.2868045

[29] Materialise, Materialise Mimics Innovation Suite. Online [Accessed 18 June 2024]
https://www.materialise.com/en/healthcare/mimics-innovation-suite

[30] Ultimaker, Ultimaker S5 and Ultimaker S5 Pro Bundle: quick start guide. Online [Accessed 18 June 2024]
https://ultimaker.my.salesforce.com/sfc/p/#j0000000HOnW/a/5b000004TWyi/KyTXfJ7VKhqF4cE6bXapRpSt98b1qrU7.beSCMA8m6U

[31] E. H. Tümer, H. Y. Erbil, Extrusion-based 3D printing applications of PLA composites: a review, Coatings 11 (2021) 4.
DOI: 10.3390/coatings11040390

[32] N. Y. Z. Ng, R. H. Abdul Haq, O. M. F. Marwah, F. H. Ho, S. Adzila, Optimization of polyvinyl alcohol (PVA) support parameters for fused deposition modelling (FDM) by using design of experiments (DOE), Mater. Today Proc. 57 (2022) 3, pp. 1226-1234.
DOI: 10.1016/j.matpr.2021.11.046

[33] A. Kalra, Developing FE human models from medical images, in: Basic Finite Element Method as Applied to Injury Biomechanics. K.-H. Yang (editor). Academic Press, 2018, pp. 389-415.
DOI: 10.1016/B978-0-12-809831-8.00009-X

[34] T. Razi, P. Emamverdizadeh, N. Nilavar, S. Razi, Comparison of the Hounsfield unit in CT scan with the gray level in cone-beam CT, J. Dent. Res. Dent. Clin. Dent. Prospects 13 (2019) 3, pp. 177-182.
DOI: 10.15171/joddd.2019.028

[35] JCGM 101:2008, Evaluation of measurement data - Supplement 1 to the Guide to the expression of uncertainty in measurement - Propagation of distributions using a Monte Carlo method, 2008.
DOI: 10.59161/JCGM101-2008

[36] G. Fiori, G. Bocchetta, S. Conforto, S. A. Sciuto, A. Scorza, Sample volume length and registration accuracy assessment in quality controls of PW Doppler diagnostic systems: a comparative study, Acta IMEKO 12 (2023) 2, pp. 1-7.
DOI: 10.21014/actaimeko.v12i2.1425

[37] G. Fiori, G. Bocchetta, M. Schmid, S. Conforto, S. A. Sciuto, A. Scorza, Novel quality assessment protocol based on Kiviat diagram for pulsed wave Doppler diagnostic systems: first results, Proc. of the 26th IMEKO TC4 International Symposium & 24th International Workshop on ADC and DAC Modelling and Testing, IMEKO TC-4 2023, Pordenone, Italy, 20 – 21 September 2023, pp. 165-169.
DOI: 10.21014/tc4-2023.38

[38] G. Fiori, F. Fuiano, M. Schmid, S. Conforto, S. A. Sciuto, A. Scorza, A comparative study on depth of penetration measurements in diagnostic ultrasounds through the adaptive SNR threshold method, IEEE Trans. Instrum. Meas. 72 (2023) 4003108, pp. 1-8.
DOI: 10.1109/TIM.2023.3250309

[39] G. Fiori, A. Pica, S. A. Sciuto, F. Marinozzi, F. Bini, A. Scorza, A comparative study on a novel quality assessment protocol based on image analysis methods for Color Doppler ultrasound diagnostic systems, Sensors 22 (2022) 24.
DOI: 10.3390/s22249868

[40] M. De Cecco, A. Luchetti, M. Tavernini, Monte Carlo human identification refinement using joints uncertainty, Acta IMEKO 12 (2023) 2, pp. 1-11.
DOI: 10.21014/actaimeko.v12i2.1423

[41] N. Covre, A. Luchetti, M. Lancini, S. Pasinetti, E. Bertolazzi, M. De Cecco, Monte Carlo-based 3D surface point cloud volume estimation by exploding local cubes faces, Acta IMEKO 11 (2022) 2, pp. 1-9.
DOI: 10.21014/acta_imeko.v11i2.1206